# NACA

# RESEARCH MEMORANDUM

FLIGHT INVESTIGATION OF THE EFFECT OF

UNDERWING PROPULSIVE JETS ON THE LIFT, DRAG, AND

LONGITUDINAL STABILITY OF A DELTA-WING CONFIGURATION

AT MACH NUMBERS FROM 1.23 TO 1.62

By Ralph A. Falanga and Joseph H. Judd

Langley Aeronautical Laboratory
Langley Field, Va.

# NATIONAL ADVISORY COMMITTEE
# FOR AERONAUTICS
## WASHINGTON

NACA RM L55I13

NATIONAL ADVISORY COMMITTEE FOR AERONAUTICS

RESEARCH MEMORANDUM

FLIGHT INVESTIGATION OF THE EFFECT OF

UNDERWING PROPULSIVE JETS ON THE LIFT, DRAG, AND

LONGITUDINAL STABILITY OF A DELTA-WING CONFIGURATION

AT MACH NUMBERS FROM 1.23 TO 1.62

By Ralph A. Falanga and Joseph H. Judd

SUMMARY

A flight test was made of a multijet 60° delta-wing airplane con-
figuration whose twin-engine exhausts were located at 18.5 percent of
the wing semispan, 38.3 percent of the root chord, and 1.5 jet diameters
below the wing mean chord line. Data were obtained for jet-on flight
conditions between Mach numbers of 1.23 and 1.29 and for jet-off flight
conditions between Mach numbers of 1.23 and 1.62. The range of Reynolds
numbers was from $23.8 \times 10^6$ to $35.0 \times 10^6$.

The drag coefficients for jet-on flight were lower than the corre-
sponding drag coefficients for jet-off flight. Although the particular
locations of the exhaust fairing reduced jet-off lift coefficients below
those which would normally be obtained for a symmetrical model, operation
of the jet increased the lift coefficients and the lift-curve slope.

Over the Mach number range for which jet-on data were obtained, the
longitudinal static-stability derivative and damping derivatives showed
little difference between jet-on and jet-off flight.

INTRODUCTION

The engine installation problem has become a major factor in the
design of supersonic airplanes. In addition to the effects of inlet
type and location on the drag and the influence of the engine location
on the airplane geometry, the propulsive jet can exert an appreciable
effect on the lift and drag of the airplane. As part of an investigation
of these problems by the Langley Pilotless Aircraft Research Division,
a study is being made of the effect of the propulsive jet on the aero-
dynamic characteristics of airplane configurations.

The problem of obtaining low-drag supersonic multi-jet bomber con-
figurations has been particularly troublesome (ref. 1), because the cross-
sectional area of the nacelles tends to concentrate at or near the max-
imum cross-sectional area of the fuselage and wing, decreasing the
effective fineness ratio of the configuration.  One solution to this prob-
lem was proposed:  namely, to locate one pair of engines in the fuselage
nose and a second pair in the fuselage tail.  Thus, the engine locations
not only improve the cross-sectional area distribution but also simplify
the problem of balancing the airplane.  This type of configuration has
shown considerable promise as a possible supersonic flying boat (ref. 2).
For these airplanes, the practical location for the forward jet exits
lies underneath the wing, thus providing a possibility of a considerable
amount of jet-induced lift at supersonic speeds (refs. 3 and 4).

The investigation reported herein was a flight test of a delta-wing
bomber configuration with two propulsive jets exhausting under the for-
ward portion of the wings.  The tests were designed to study the effect
of the propulsive jet on the drag, lift, and trim characteristics of
this configuration and to compare measured values of lift and trim changes
between jet-on and jet-off flight with predicted values obtained from
the action of a jet on a flat plate at zero angle of attack.

The propulsive jet issuing from twin sonic exhaust nozzles simulated
the exhaust parameters of a current turbojet at an altitude of 35,000
feet and a Mach number of 1.5 by utilizing a solid-propellant rocket
motor designed according to reference 5.

The flight test was made at the Langley Pilotless Aircraft Research
Station at Wallops Island, Va.  The Mach number range of these tests was
from 1.23 to 1.62 and the Reynolds number range from $23.8 \times 10^6$ to
$35.0 \times 10^6$.

## SYMBOLS

$A$        cross-sectional area of any longitudinal station, sq ft

A.C.     distance from leading edge of mean aerodynamic chord to aero-
             dynamic center of model, percent of mean aerodynamic chord,
             positive rearward

$C_D$       drag coefficient,  Drag/qs

$C_L$       lift coefficient,  Lift/qs

$C_{L_\alpha}$       slope of lift curve, $dC_L/d\alpha$, per deg

$C_{L_T}$       trim lift coefficient

$C_m$     pitching-moment coefficient, with respect to center of gravity,

$$\frac{\text{Pitching moment}}{qS\bar{c}}$$

$C_{m_\alpha}$     static-stability derivative, $\dfrac{dC_m}{d\alpha}$, per deg

$C_{m_{\dot{\alpha}}} = \dfrac{\partial C_m}{\partial\left(\dfrac{\dot{\alpha}\bar{c}}{2V}\right)}$    per radian

$C_{m_q} = \dfrac{dC_m}{d\left(\dfrac{\dot{\theta}\bar{c}}{2V}\right)}$    per radian

$C_{m_q} + C_{m_{\dot{\alpha}}}$    longitudinal damping derivatives, per radian

$\bar{c}$     wing mean aerodynamic chord, ft

$c_p$     wing static-pressure coefficient, $\dfrac{p_w - p_o}{q}$

$c_{p_T}$     trim wing static-pressure coefficient

$l$     fuselage length, ft

$M$     Mach number, $\dfrac{V}{\text{Speed of sound}}$

$P$     period, sec

$p$     static pressure, lb/sq ft

$q$     dynamic pressure, lb/sq ft

$R$     Reynolds number (based on mean aerodynamic chord)

$r$     radius of equivalent body of revolution, ft

$S$     wing area (including the area enclosed within the fuselage), sq ft

$T_{1/2}$     time required for short-period oscillation to damp to one-half amplitude, sec

t        time, sec

V        velocity of flight, ft/sec

x        distance along fuselage center line measured from nose, ft

$z/d_j$   distance below wing surface in jet diameters

α        angle of attack, measured from fuselage reference line, deg

$\dot{\alpha} = \dfrac{1}{57.3}\dfrac{d\alpha}{dt}$, radians/sec

$\alpha_T$      trim angle of attack, deg

θ        angle of pitch, measured from fuselage reference line, radians

$\dot{\theta} = \dfrac{d\theta}{dt}$, radians/sec

Subscripts:

o        free-stream condition

j        jet

w        wing

## MODEL AND APPARATUS

### Model

A three-view drawing of the flight model is shown in figure 1 and the basic geometric parameters are tabulated in table I. The basic configuration consisted of a triangular wing with 60° sweepback on the leading edge and 10° sweepforward on the trailing edge, mounted on a body of revolution whose ordinates are given in table II. The wing, 10.67 square feet in total plan-form area, had an NACA 65A004 airfoil section and was faired to the fuselage by modified triangular fillets, as shown in figure 1. Two hexagonal airfoil fins 2.5 percent thick at the root were used for vertical fins. Three pulse rockets were located in the nose to disturb the model in pitch.

The general location of the engine jet fairing is shown in figure 1. Detail dimensions of the fairing and nozzles are shown in figure 2(a).

Basically, the fairing consists of a pointed nose, a straight section, and a circular conical boattail of 7.5° half-angle. Figure 2(b) is a photograph of the engine nozzle and fairing viewed from the bottom rear. A photograph of the model showing the engine fairings is given in figure 3. The cross-sectional area distribution of the complete configuration is shown in figure 4 together with its equivalent body of revolution.

The basic turbojet simulator utilized in this model consisted of a combustion chamber, a flow-control nozzle, a plenum chamber, and twin convergent sonic exit sections. A standard cordite SU/K propellant grain generated the necessary exhaust gases to simulate current full-scale turbojet exhaust parameters. (See ref. 5.) The jet-exit diameter was 2.60 inches and the jet-base diameter was 2.75 inches, corresponding to a jet area of 0.0369 square foot and a jet-base area of 0.0415 square foot. Weight, center of gravity, and moment of inertia for the model with and without rocket fuel are presented in table III.

## Model Instrumentation

A six-channel telemeter which was carried in the nose of the model continuously transmitted measurements of free-stream total pressure, angle of attack, longitudinal and normal acceleration, combustion-chamber pressure, and wing static pressure. The wing static-pressure orifice was located on the bottom of the wing as shown in figure 1. The normal accelerometer was located at station 32.56, 19.60 inches forward of the initial center of gravity.

The rocket-motor combustion-chamber pressure instrument and telemeter were checked in a preflight motor firing in the Langley rocket test cell. Using the data from this test a calibration curve of the rocket thrust, exhausting into a vacuum, as a function of the combustion-chamber pressure was obtained.

Data for the flight tests were obtained by use of telemeter, CW Doppler velocimeter, tracking radar, and radiosonde. The radiosonde gave a survey of the atmospheric conditions over the test altitude. The model velocity obtained with the velocimeter was corrected for wind velocity which was determined from rawinsonde measurements.

## FLIGHT TESTS

The model was launched from a mobile launcher (fig. 3). Two ABL Deacon rocket motors boosted the configuration to the peak Mach number. Jet-off data were obtained during the decelerating flight after separation of the model from the booster. Jet-on data were obtained

during firing of the turbojet simulator which was started at the lowest
test Mach number.  The limited Mach number range of jet-on data was a
byproduct of low acceleration caused by high model drag and the low
scale thrust.  During jet-off flight a pulse rocket disturbed the model
in pitch, and a disturbance in pitch was also obtained when the turbojet
simulator motor fired.  The variation of Reynolds number based on wing
mean aerodynamic chord with Mach number for jet-on and jet-off flight
is presented in figure 5.

The angle of attack and normal accelerometer data were corrected
to the model center of gravity.  The method of obtaining jet-on and jet-
off drag data was explained in reference 6 and the method of determining
lift and longitudinal stability data from transient disturbances in
pitch is given in reference 7.  All lift coefficients presented have had
the lift component due to the jet subtracted, except where otherwise
stated.

## RESULTS AND DISCUSSION

### Effect of Jet on Drag

The variation of drag coefficients with angle of attack for jet-on
and jet-off conditions is shown in figure 6.  The data presented for
jet-on flight were at an average Mach number of 1.23, whereas those for
jet-off flight were at an average Mach number of 1.31.  These data indi-
cate that the angle of attack for minimum drag coefficient increases by
approximately one-half of a degree from jet-on to jet-off flight.  The
variation of drag coefficient at trim angle of attack with Mach number
is presented in figure 7 and the variation of trim angle of attack with
Mach number is presented in figure 8.

From the drag coefficients of figure 7, it can be seen that the
jet-on drag coefficients are lower than the jet-off drag coefficients.
The small change in trim angle of attack due to the jet does not change
the drag coefficient by an appreciable amount.  Furthermore the approx-
imate difference between jet-on and jet-off engine base drag coefficient
(based on total wing area) obtained from reference 6 was 0.0006 at Mach
numbers from 1.23 to 1.31.  The measured difference between jet-on and
jet-off drag coefficients is considerably greater than this difference
in base drag coefficient and that due to the change in trim angle of
attack.  The reduction of drag coefficient between jet-off and jet-on
flight is caused by jet effects such as positive pressure increments
acting on the boattail or by the jet acting favorably on the complete
configuration.

Exhaust and wing fairings were designed from the standpoint of simple geometry and construction instead of low drag. Hence, comparison of the drag coefficients of this configuration with similar multijet configurations (ref. 1) indicates that the supersonic drag coefficient is comparatively high.

## Jet Effect on Lift

The variations of lift coefficient with angle of attack for jet-on flight at a Mach number of 1.23 and for jet-off flight at a Mach number of 1.31 are plotted in figure 9. Included in the values for jet-on lift coefficients is the upward thrust component of the propulsive jet. The lift coefficient due to the upward thrust component was subtracted from the measured lift coefficients of figure 9 to obtain the lift coefficient of the configuration including the increment due to the pressure field of the propulsive jet. These jet-on lift coefficients are plotted in figure 10. Since the measured lift coefficients for jet-off flight were obtained at an average Mach number of 1.31, the jet-off lift-curve slope was corrected to that of Mach number 1.23 by using the ratio of lift-curve slopes for an aspect-ratio-2 triangular-wing and body combination at the respective Mach numbers (ref. 8). This increased the lift-curve slope from 0.0407 at a Mach number of 1.31 to 0.0415 at a Mach number of 1.23. This value of lift-curve slope was plotted in figure 10 through the trim lift coefficient and trim angle of attack. It is apparent that operation of the jet has increased both the lift-curve slope and the lift coefficients. Also it may be noted that the exhaust fairings have reduced the lift coefficients below those which would normally be obtained with a symmetrical model.

The experimental values of lift-curve slope are plotted in figure 11, together with data from references 8 and 9 for an aspect-ratio-2 delta wing located in a midwing position. The exhaust fairings have reduced the jet-off lift-curve slope below that of the symmetrical models. Although part of the difference may be due to wing elasticity, an appreciable portion of the reduction in lift-curve slope is believed due to the exhaust fairings and nozzle location. The effect of the jet was favorable over the angle-of-attack range and Mach number values for which data were obtained.

The trim lift coefficient for jet-on and jet-off flight is given in figure 12. The change in trim angle of attack between jet-on and jet-off flight (fig. 8) was small. Thus, the large difference in trim lift coefficient was attributable to the increment in wing lift caused by the jet pressure field.

Although there were no experimental data for the jet-induced incremental lift for the Mach number range of the flight test, unpublished

data on the jet-induced incremental pressures on a flat plate at $0^\circ$ angle of attack and at a Mach number of 1.39 were available. Assuming that this incremental pressure distribution acted on the delta wing, integration of the distributions gives the change in lift coefficients between jet-on and jet-off flight. These results are shown in figure 13 as a function of jet distance below the wing surface. Incremental lift coefficients for the flat plate varied from 0.039 to 0.053, while the incremental lift coefficient for the present configuration was 0.044. The results of this flight test show, therefore, that at zero angle of attack, the change in lift coefficient between jet-on and jet-off flight can be reasonably estimated from data on the pressure field on a flat plate induced by an exhaust jet.

The variation of jet-exit static-pressure ratio $p_j/p_o$ and wing trim static-pressure coefficients is presented in figures 14 and 15, respectively. The variations of wing static-pressure coefficient with angle of attack at Mach numbers of 1.59 and 1.31 for jet-off flight and at a Mach number of 1.23 for jet-on flight are plotted in figure 16. These data show that a positive increment in pressure coefficient between jet-off and jet-on conditions was obtained at the wing static-pressure orifice. References 3 and 4 also show that for the same relative position from nacelle exit a positive increment in pressure coefficient occurred at zero angle of attack.

## Static Longitudinal Stability

The period of the longitudinal oscillations of the angle of attack is given in figure 17. The period was used to compute the static-stability derivative $C_{m_\alpha}$ which is shown in figure 18. Although a very limited amount of data was obtained from these tests, the static-stability derivative appears insensitive to jet action. The aerodynamic center (fig. 19) computed by using experimental values of $C_{m_\alpha}$ and $C_{L_\alpha}$ also appears insensitive to jet operation.

The change in trim angle of attack due to the jet operation (fig. 8) was nearly equal to that required to compensate for the thrust eccentricity of the jet engines. The computed change in trim angle due to the thrust eccentricity was 0.61, while the measured trim change at a Mach number of 1.23 was 0.50. It should be reemphasized that a very small Mach number range was covered and at higher Mach numbers the jet may exert a greater influence on trim angle of attack.

## Dynamic Longitudinal Stability

The time required for the short-period longitudinal oscillation to damp to one-half amplitude is shown in figure 20 and the damping derivatives $(C_{m_q} + C_{m_{\dot{\alpha}}})$ are shown in figure 21. The effect of jet operation on the damping derivatives appears to be small at the Mach number for which jet-on data were obtained. The jet-off data indicate that the model had more damping at a Mach number of 1.59 than at a Mach number of 1.3 or 1.23. Also plotted in figure 21 are theoretical values of damping derivatives for this model, computed by the method of reference 10, and experimental values of damping derivatives obtained from reference 9. Reference 9 indicates fair agreement with the theoretical values plotted, whereas the experimental values of damping derivatives from this test indicate lower damping than the theoretical values for the lower test Mach numbers and higher damping at a Mach number of 1.58.

## CONCLUDING REMARKS

A flight test of a twin-jet delta-wing bomber was made between Mach numbers of 1.23 and 1.62 and Reynolds numbers of $23.8 \times 10^6$ and $35.0 \times 10^6$. Data obtained during flight tests with the jet operating (at Mach numbers from 1.23 to 1.29) and with no jet indicated the following conclusions:

1. The jet-on drag coefficients of the configuration were lower than the jet-off drag coefficients.

2. The jet-on lift coefficients and lift-curve slope were larger than the jet-off values at corresponding angles of attack. It appears that the incremental lift coefficients can be reasonably estimated from the incremental lift produced by jet effects on a flat plate at zero angle of attack.

3. The installation of the exhaust nozzles and their fairings reduced the lift coefficients for the jet-off case from that which normally would be expected from a symmetrical model at zero angle of attack.

4. The static and dynamic longitudinal stability derivatives were apparently affected very slightly by the operation of the jet.


Langley Aeronautical Laboratory,
    National Advisory Committee for Aeronautics,
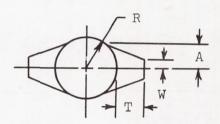        Langley Field, Va., September 12, 1955.

REFERENCES

1. Hall, James Rudyard:  Comparison of Free-Flight Measurements of the
     Zero-Lift Drag Rise of Six Airplane Configurations and Their
     Equivalent Bodies of Revolution at Transonic Speeds.  NACA
     RM L53J21a, 1954.

2. Olson, Roland E., and Bielat, Ralph P.:  An Aerodynamic and
     Hydrodynamic Investigation of Two Multijet Water-Based Aircraft
     Having Low Transonic Drag Rise.  NACA RM L55A11a, 1955.

3. Bressette, Walter E.:  Investigation of the Jet Effects on a Flat
     Surface Downstream of the Exit of a Simulated Turbojet Nacelle at
     a Free-Stream Mach Number of 2.02.  NACA RM L54E05a, 1954.

4. Bressette, Walter E., and Faget, Maxime A.:  An Investigation of Jet
     Effects on Adjacent Surfaces.  NACA RM L55E06, 1955.

5. de Moraes, Carlos A., Hagginbotham, William K., Jr., and Falanga,
     Ralph A.:  Design and Evaluation of a Turbojet Exhaust Simulator,
     Utilizing a Solid-propellant Rocket Motor, for Use in Free-Flight
     Aerodynamic Research Models.  NACA RM L54I15, 1954.

6. Falanga, Ralph A.:  A Free-Flight Investigation of the Effects of
     Simulated Sonic Turbojet Exhaust on the Drag of a Boattail Body
     With Various Jet Sizes From Mach Numbers 0.87 to 1.50.  NACA
     RM L55F09a, 1955.

7. Gillis, Clarence L., Peck, Robert F., and Vitale, A. James:
     Preliminary Results From a Free-Flight Investigation at Transonic
     and Supersonic Speeds of the Longitudinal Stability and Control
     Characteristics of an Airplane Configuration With a Thin Straight
     Wing of Aspect Ratio 3.  NACA RM L9K25a, 1950.

8. Hall, Charles F.:  Lift, Drag, and Pitching Moment of Low-Aspect-
     Ratio Wings at Subsonic and Supersonic Speeds.  NACA RM A53A30,
     1953.

9. D'Aiutolo, Charles T.:  Low-Amplitude Damping-in-Pitch Characteristics
     of Tailless Delta-Wing—Body Combinations at Mach Numbers From 0.80
     to 1.35 As Obtained With Rocket-Powered Models.  NACA RM L54D29,
     1954.

10. Henderson, Arthur, Jr.:  Pitching-Moment Derivatives  $C_{m_q}$  and $C_{m_{\dot{\alpha}}}$
     at Supersonic Speeds for a Slender-Delta-Wing and Slender-Body
     Combination and Approximate Solutions for Broad-Delta-Wing and
     Slender-Body Combinations.  NACA TN 2553, 1951.

TABLE I.- GEOMETRIC CHARACTERISTICS OF MODEL TESTED

Fuselage:
    Fineness ratio of equivalent body of revolution . . . . . .   8.23
    Total frontal area, sq ft  . . . . . . . . . . . . . . . . .  0.5535
    Base area, sq ft . . . . . . . . . . . . . . . . . . . . .  0.1806

Wing:
    Aspect ratio . . . . . . . . . . . . . . . . . . . . . .   2.10
    Taper ratio . . . . . . . . . . . . . . . . . . . . . . . .     0
    Mean aerodynamic chord, ft . . . . . . . . . . . . . .   3.01
    Airfoil section . . . . . . . . . . . . . . . . . . .  NACA 65A004
    Total plan-form area, sq ft . . . . . . . . . . . . . . . .  10.67

Engine fairing (for one fairing):
    Projected frontal area, sq ft . . . . . . . . . . . . . . .  0.347
    Base area, sq ft  . . . . . . . . . . . . . . . . . . . .  0.0415
    Jet-exit area, sq ft  . . . . . . . . . . . . . . . . . .  0.0369

Vertical tail (both fins):
    Area (extended to center line), sq ft  . . . . . . . . .  2.176
    Aspect ratio . . . . . . . . . . . . . . . . . . . . . . .  1.458
    Taper ratio,  Tip chord/Root chord. . . . . . . . . . . .  0.169
    Airfoil section . . . . . . . . . . . . . . . . . .  Hexagonal airfoil

## TABLE II.- FUSELAGE ORDINATES

[All dimensions in inches.  All letter dimensions defined
in the sketch apply only to this table]



| x | R | T | W | A |
|---|---|---|---|---|
| 0 | 0 | ----- | ----- | ----- |
| .875 | .168 | ----- | ----- | ----- |
| 1.120 | .224 | ----- | ----- | ----- |
| 2.100 | .460 | ----- | ----- | ----- |
| 5.675 | 1.245 | ----- | ----- | ----- |
| 10.675 | 2.155 | ----- | ----- | ----- |
| 15.575 | 2.785 | ----- | ----- | ----- |
| 20.475 | 3.220 | ----- | ----- | ----- |
| 25.375 | 3.500 | ----- | ----- | ----- |
| 31.075 | 3.500 | 0 | 0 | 0 |
| 35.063 | 3.500 | .906 | 1.188 | 2.650 |
| 78.308 | 3.500 | .906 | 1.188 | 2.650 |
| 78.683 | 3.437 | .935 | 1.170 | 2.610 |
| 79.683 | 3.268 | .830 | 1.020 | 2.320 |
| 80.683 | 3.099 | .655 | .770 | 1.930 |
| 81.683 | 2.930 | .380 | .440 | 1.410 |
| 82.933 | 2.875 | 0 | 0 | 0 |

TABLE III.- PHYSICAL CHARACTERISTICS OF MODEL TESTED

| Characteristic | Jet off | Jet on | |
|---|---|---|---|
| | | M = 1.23 | M = 1.28 |
| Weight, lb . . . . . . . . | 199.25 | 197.55 | 190.47 |
| Center-of-gravity position, percent of $\bar{c}$ . . . . . . | 29.78 | 29.60 | 28.75 |
| Moment of inertia in pitch about center of gravity, slug-ft$^2$ . . . . . . . . | 11.0446 | 10.936 | 10.698 |

Total pressure tube

Fus. sta.
0

61.561

18.500

60°

.313

3.000

15.170

1.000

10.50°

43.813

82.938

A

A

Jet exhaust nozzle
and fairing

3.994

35.75°

5.258

28.378

Angle of attack indicator

Wing static
pressure orifice

3.750 rad.

10°

25.010

24.862

54.167

60°

10°  5.549

5.750 diam.

9.450

c̄

41.410

4.406

2.376  7.000 diam.

Section AA
Fuselage and fillet
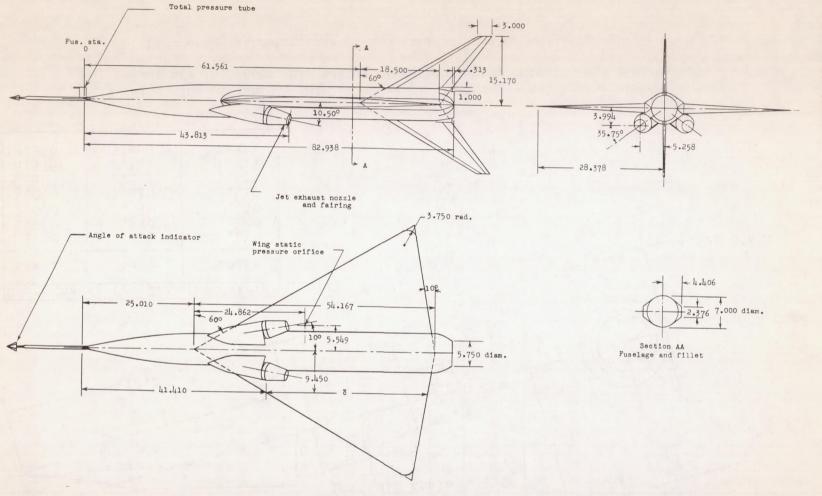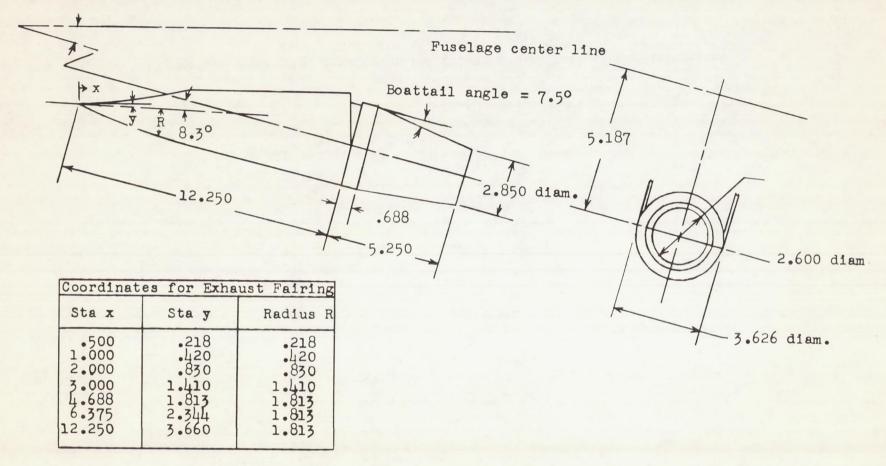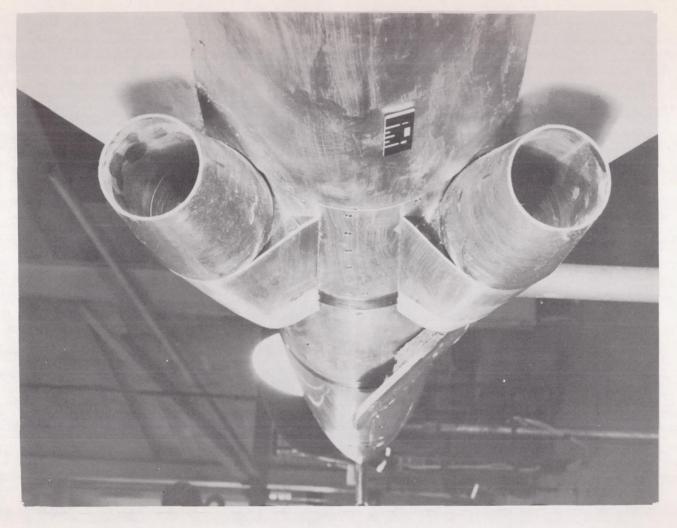
Figure 1.- Three-view drawing of the flight model.  All linear dimensions
are in inches.

Fuselage center line

Boattail angle = 7.5°

x

y   R

8.3°

12.250

.688

5.250

2.850 diam.

5.187

2.600 diam.

3.626 diam.

| Coordinates for Exhaust Fairing | | |
|---|---|---|
| Sta x | Sta y | Radius R |
| .500 | .218 | .218 |
| 1.000 | .420 | .420 |
| 2.000 | .830 | .830 |
| 3.000 | 1.410 | 1.410 |
| 4.688 | 1.813 | 1.813 |
| 6.375 | 2.344 | 1.813 |
| 12.250 | 3.660 | 1.813 |

(a) Side view of exhaust nozzles and engine fairing.  All linear dimen-
sions are in inches; all letter dimensions apply only to this figure.

Figure 2.- Illustrations of the exhaust nozzles and fairings.

(b) Rear view of exhaust nozzles and engine fairings.

Figure 2.- Concluded.

L-87997
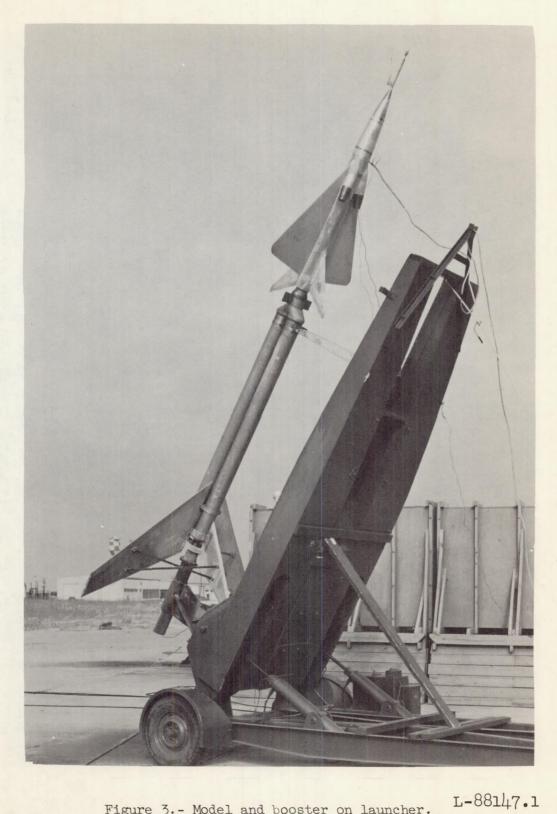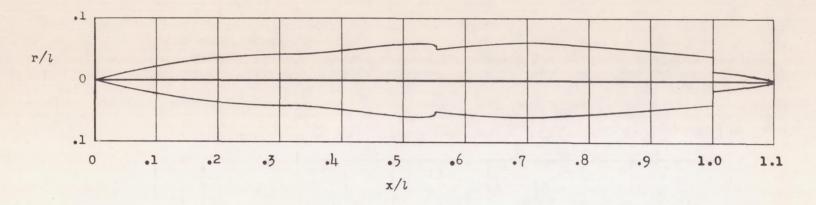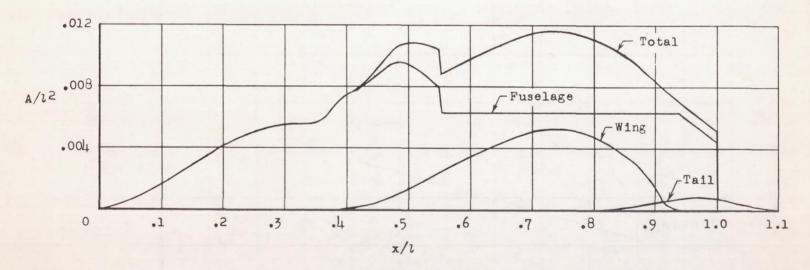
Figure 3.- Model and booster on launcher.                L-88147.1

(a) Equivalent body of revolution.   Fineness ratio, 8.23.



(b) Cross-sectional area distribution.

Figure 4.- The cross-sectional area distribution and equivalent body of
revolution for the model.
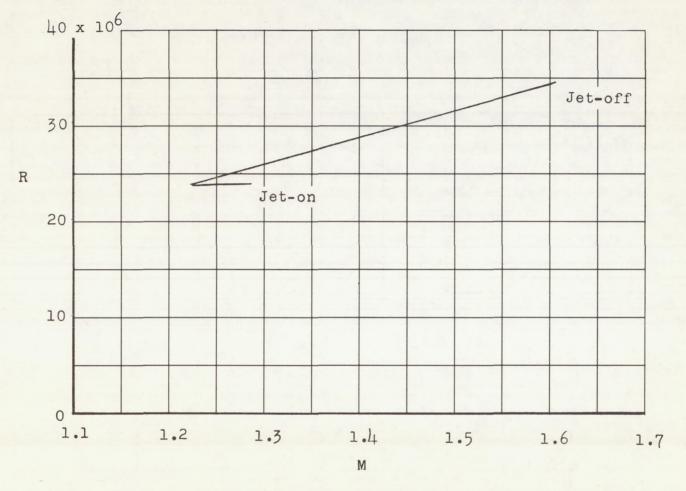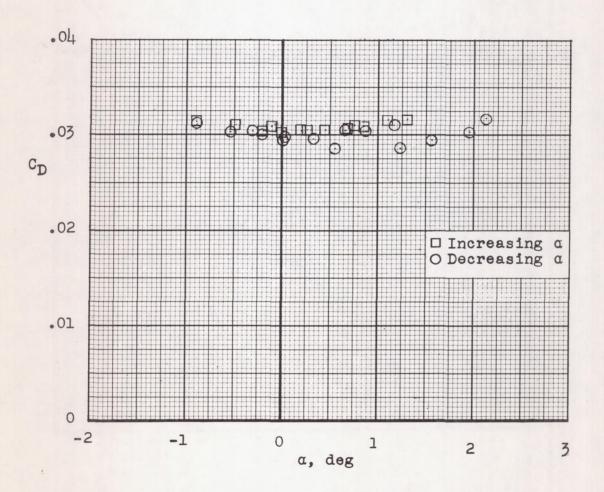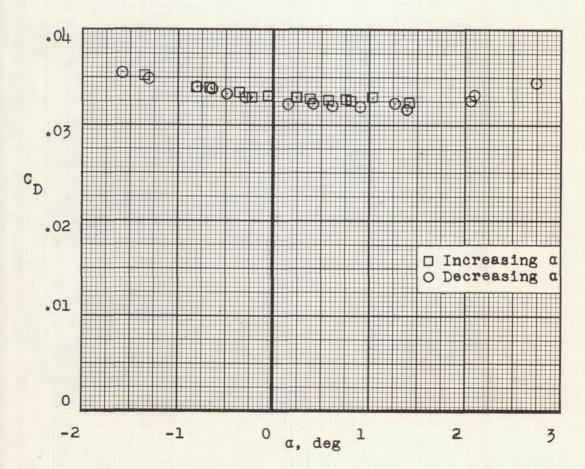
Figure 5.- The variation of Reynolds number with Mach number for jet-on and jet-off flight. Values of Reynolds number are based on the wing mean aerodynamic chord.

(a) Jet-on flight at an average Mach number of 1.23.

Figure 6.- Variation of drag coefficients with angle of attack.

(b) Jet-off flight at an average Mach number of 1.31.

Figure 6.- Concluded.
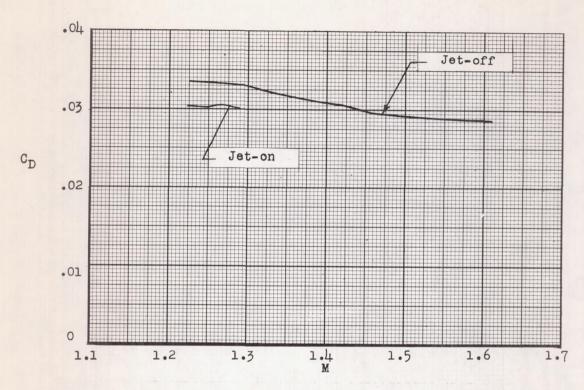
Figure 7.- Variation of trim drag coefficient with Mach number.
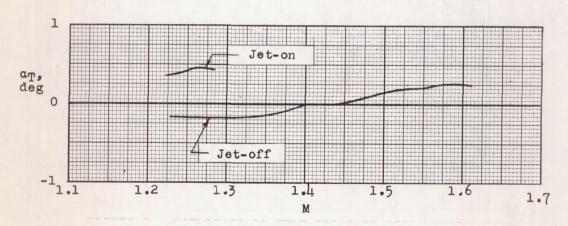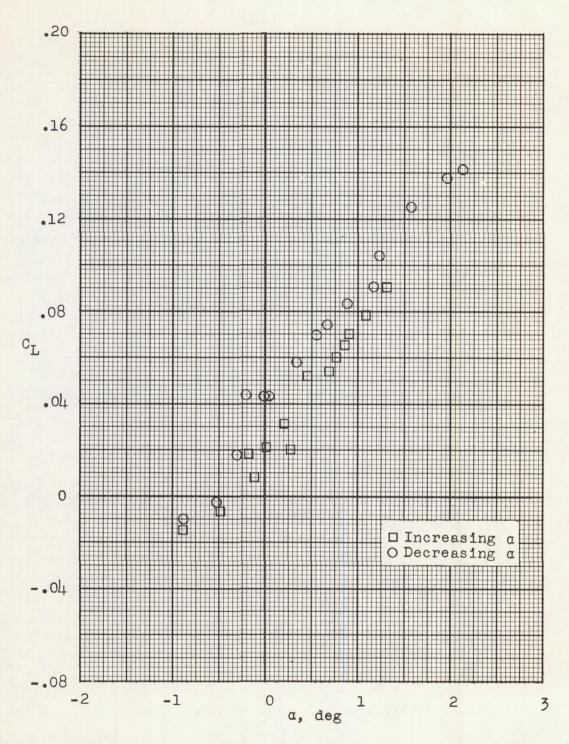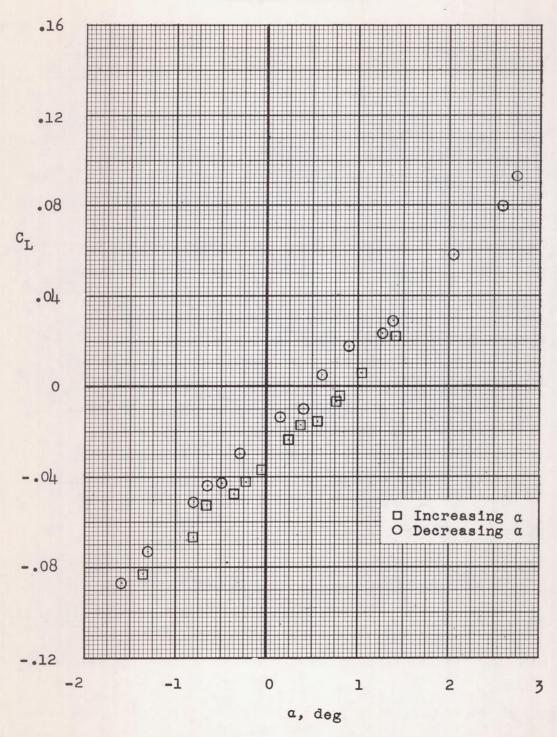


Figure 8.- Variation of trim angle of attack with Mach number.

(a) Variation of lift coefficient with angle of attack for jet-on flight at an average Mach number of 1.23.

Figure 9.- Lift coefficients obtained during the oscillating parts of the flight.

(b) Variation of lift coefficient with angle of attack for jet-off flight at an average Mach number of 1.31.

Figure 9.- Concluded.
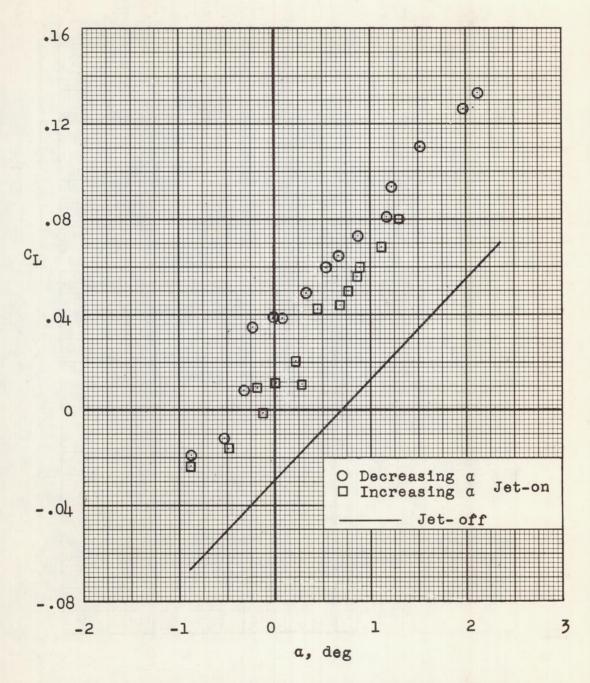
Figure 10.- A comparison of jet-on and jet-off lift coefficients at a
Mach number of 1.23.
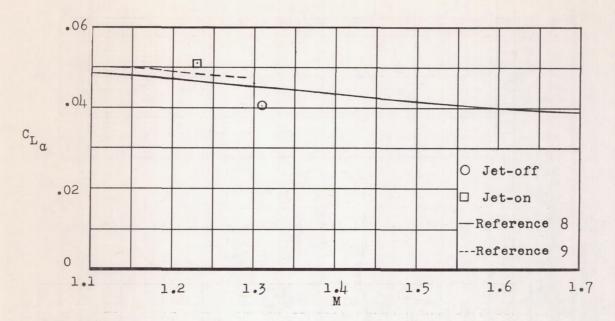
Figure 11.- Comparison of lift-curve slope with Mach number.
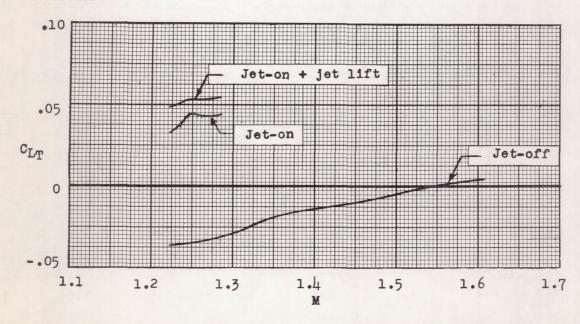


Figure 12.- Variation of trim lift coefficient with Mach number.
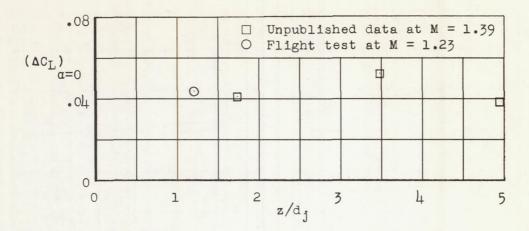
Figure 13.- The variation of jet-induced incremental lift coefficients with jet distance from the wing.
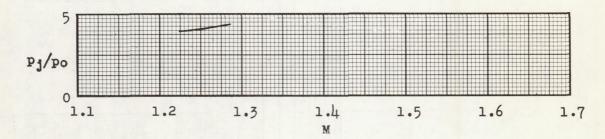


Figure 14.- Variation of jet-exit static-pressure ratio with Mach number.
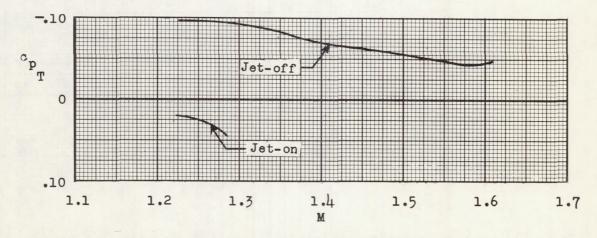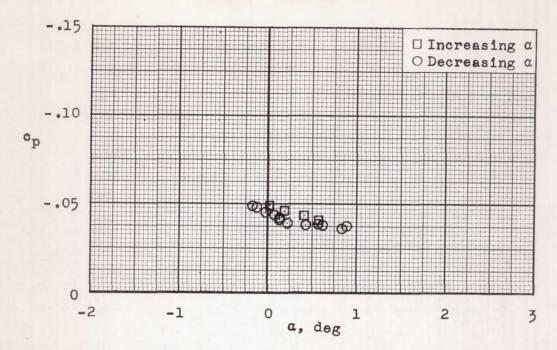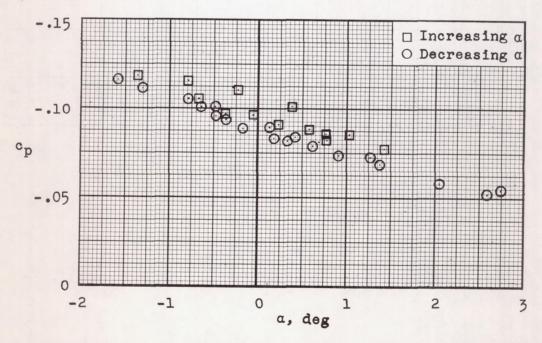


Figure 15.- Variation of wing static-pressure coefficient with Mach number at trim angle of attack.
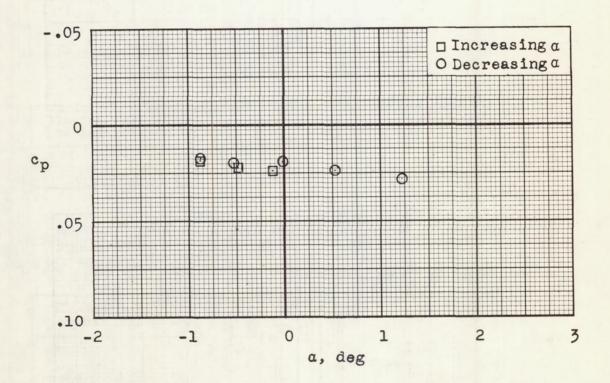
(a) Jet-off wing pressure coefficient at Mach number 1.59.



(b) Jet-off wing pressure coefficient at Mach number 1.31.

Figure 16.- Variation of wing static-pressure coefficient with angle of
attack.

(c) Jet-on wing pressure coefficient at Mach number 1.23.

Figure 16.- Concluded.
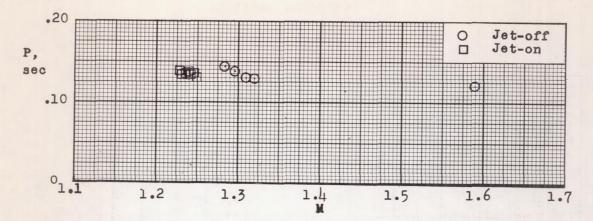
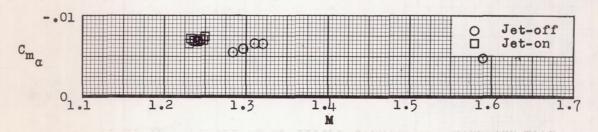Figure 17.- Variation of the period of the short-period oscillation with Mach number for jet-on and jet-off flight.



Figure 18.- Variation of static-stability derivative with Mach number for jet-off and jet-on flight.
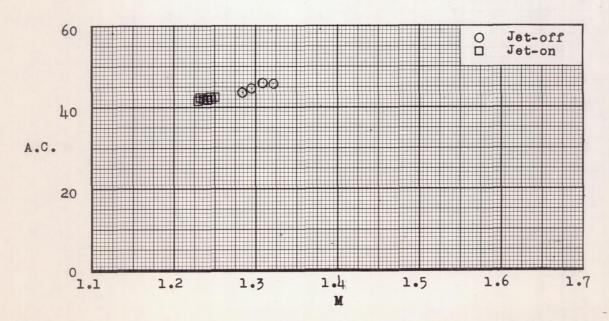


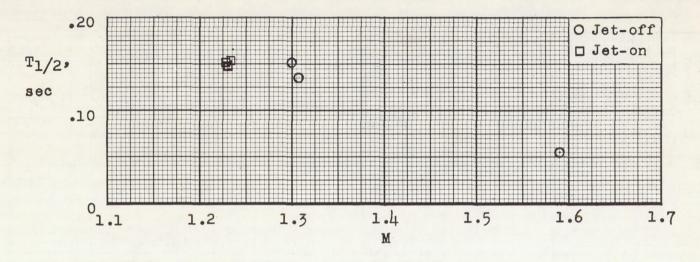Figure 19.- Variation of aerodynamic-center location with Mach number for jet-off and jet-on flight.

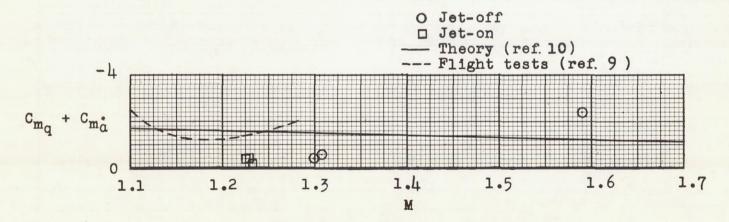Figure 20.- Variation of time to damp to one-half amplitude for jet-on
and jet-off flight.



Figure 21.- Variation of jet-on and jet-off damping derivatives with
Mach number.